

Cobalt(II) Ions Connecting $[\text{Co}^{\text{II}}_4]$ Helicates into a 2-D Coordination Polymer Showing Slow Relaxation of the Magnetization

Paula Cucos,[†] Lorenzo Sorace,^{*,‡,§} Catalin Maxim,[§] Sergiu Shova,^{||} Delia Patroi,[⊥] Andrea Caneschi,[‡] and Marius Andruh^{*,§,||}

[†]Ilie Murgulescu-Institute of Physical Chemistry of the Romanian Academy, Splaiul Independentei no. 202, 060021 Bucharest, Romania

[‡]Department of Chemistry "U. Schiff" and INSTM RU, University of Florence, Via della Lastruccia 3, 50019 Florence, Italy

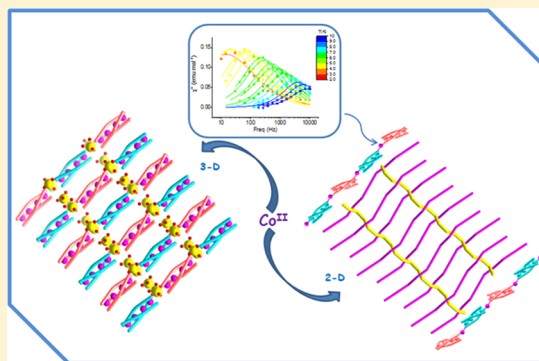
[§]University of Bucharest, Faculty of Chemistry, Inorganic Chemistry Laboratory, Str. Dumbrava Rosie no. 23, 020464 Bucharest, Romania

^{||}Petru Poni, Institute of Macromolecular Chemistry, Aleea Grigore Ghica Voda 41A, RO-700487 Iasi, Romania

[⊥]National Institute for R&D in Electrical Engineering INCDIE ICPE-CA, Splaiul Unirii no. 313, 030138 Bucharest, Romania

Supporting Information

ABSTRACT: The reactions of cobalt(II) perchlorate with a diazine tetratopic helicand, H_4L , in the presence of sodium carbonate afford two coordination polymers constructed from tetranuclear anionic helicates as building blocks: $\infty^3[\text{Co}_4\text{L}_3\text{Na}_4(\text{H}_2\text{O})_4] \cdot 4\text{H}_2\text{O}$ (**1**) and $\infty^2[\text{Co}_5\text{L}_3\text{Na}_2(\text{H}_2\text{O})_9] \cdot 2.7\text{H}_2\text{O} \cdot \text{DMF}$ (**2**). The tetranuclear triple-stranded helicates, $\{\text{Co}^{\text{II}}_4\text{L}_3\}^{4-}$, are connected in **1** by sodium(I) ions and in **2** by sodium(I) and cobalt(II) ions (H_4L results from the condensation reaction between 3-formylsalicylic acid and hydrazine). The crystal structures of the two compounds have been solved. In both compounds the anionic helicates interact with the assembling cations through the carboxylato oxygen atoms. Compound **2** features chains resulting from connecting the tetranuclear helicates through cobalt(II) ions. The analysis of the magnetic properties of compounds **1** and **2** evidenced a dominant antiferromagnetic coupling for **1**, resulting in a diamagnetic ground state. In contrast, the magnetic behavior of **2** is dominated at low temperature by the Co^{II} ion which connects the antiferromagnetically coupled $\{\text{Co}^{\text{II}}_4\}$ helical moieties. The ac magnetic measurements for **2** reveal the occurrence of slow relaxation of the magnetization that is due to the single, uncorrelated cobalt(II) ions, which are diluted in an essentially diamagnetic matrix of $\{\text{Co}^{\text{II}}_4\}$ moieties ($\Delta E_{\text{eff}} = 26.7 \pm 0.3 \text{ cm}^{-1}$ with $\tau_0 = (2.3 \pm 0.2) \times 10^{-6} \text{ s}$).



INTRODUCTION

The helicates represent an important chapter in metallosupramolecular chemistry.^{1–10} Their rational design consists of metal-directed self-assembly processes using programmed ligands (helicands), which are linear strands with repeating complexation sites, separated by spacers characterized by a limited flexibility.^{11,12} The helicands are twisted as a result of the interaction with the metal ions. Beyond their beauty, the metallohelicates display exciting physical properties, such as luminescence^{13–15} and magnetism.^{16–24} In the field of crystal engineering, numerous coordination polymers featuring helical chains have been described.²⁵ On the other hand, the construction of coordination polymers using discrete helicates as building blocks is limited to a few examples.^{26–28} In principle, the helicates can be incorporated into a coordination polymer in two ways: (a) through additional metal ions, that are coordinated by the potentially bridging groups of anionic helicates, and (b) through additional anions which bridge the terminal metal ions of cationic helicates.

An easily accessible class of helicands is represented by diazine molecules, which are obtained from condensation reactions between keto precursors and hydrazine.^{29–32} Such a ligand was obtained by us from 3-formylsalicylic acid and hydrazine (H_4L)³³ and acts as a heterotetratopic helicand. That is, it contains four binding domains: two with only O donor atoms and two others with N and O donor atoms. The different coordination sites also make this ligand appropriate for obtaining heterometallic helicates. Indeed, the reaction of H_4L , cobalt(II) perchlorate, iron(III) perchlorate, and sodium carbonate afforded triple-stranded tetranuclear anionic helicates, $[\text{L}_3\text{Co}^{\text{II}}_2\text{Fe}^{\text{III}}_2]^{2-}$, which are connected through sodium ions, resulting in infinite chiral chains. In other words, the discrete anionic helicates can generate coordination polymers if they are linked by another metal ion, which is coordinated by the peripheral carboxylato oxygen atoms. This result prompted us to check the possibility of

Received: June 27, 2017

Table 1. Crystallographic Data and Details of Data Collection and Structure Refinement Parameters

	1	2
chem formula	C ₄₈ H ₄₀ Co ₄ N ₆ Na ₄ O ₂₆	C ₅₁ H _{54.4} Co ₃ N ₇ Na ₂ O _{30.7}
formula wt (g/mol)	1444.55	1597.25
cryst syst	orthorhombic	monoclinic
space group	<i>Abm2</i>	<i>P2₁/n</i>
<i>a</i> (Å)	17.9377(3)	21.1009(11)
<i>b</i> (Å)	33.2486(4)	12.3163(12)
<i>c</i> (Å)	9.8599(1)	23.047(2)
α (deg)	90.00	90.00
β (deg)	90.00	102.64(6)
γ (deg)	90.00	90.00
<i>V</i> (Å ³), <i>Z</i>	5880.48(14), 8	5844.9(8), 4
temp (K)	293(2)	160
calcd density (Mg m ⁻³)	1.613	1.815
abs coeff (mm ⁻¹)	1.227	1.508
no. of rflns collected	21223	27152
no. of indep rflns	5198 (<i>R</i> _{int} = 0.065)	9960 (<i>R</i> _{int} = 0.1812)
no. of data/restraints/params	5198/1/404	9960/30/867
final <i>R</i> indices (<i>I</i> > 2σ(<i>I</i>))		
<i>R</i> 1	0.0764	0.0797
<i>wR</i> 2	0.2006	0.1121
<i>R</i> indices (all data)		
<i>R</i> 1	0.1031	0.1917
<i>wR</i> 2	0.2316	0.1495
goodness of fit on <i>F</i> ²	1.013	0.933
$\Delta\rho_{\max}$ and $\Delta\rho_{\min}$ (e Å ⁻³)	1.239 and -0.775	0.774 and -0.626

connecting the anionic helicates with paramagnetic metal ions, in order to obtain extended networks with interesting magnetic properties. Among these, we mention the possibility of observing slow relaxation of the magnetization and then magnetic bistability, as a consequence of either 1D Ising type magnetic behavior (single-chain magnetism)³⁴ or single-molecule magnetism due to the anisotropy of a single ion, resulting in a barrier to magnetization reversal, often termed single ion magnet (SIM).^{35,36} Most of the helicates featuring the latter behavior are based on strongly anisotropic lanthanide cations.^{13,14} In this respect, it is tempting to try using Co^{II}, a largely anisotropic ion, as a building unit for helicate-based SIMs. We had some success along this line by including tetrahedral Co^{II} in *o*-vanillin-based helicates,¹⁵ resulting in a dinuclear helicate showing slow relaxation of the magnetization in applied field. On the other hand, the use of octahedral Co^{II} to obtain SIM helicates has not been reported to date. Given the large anisotropy of this ion, this might appear surprising at first sight. However, one should consider that for octahedral Co^{II} slow relaxation dynamics only arises as a consequence of a subtle interplay of ligand field and hyperfine and dipolar interactions.³⁷ As such, the actual mechanism of relaxation is often not easily determined, and slow dynamics has been observed for systems characterized by very different anisotropic features, ranging from easy plane to rhombic and easy axis.^{38–46}

Finally, the design of a chiral paramagnetic system is in principle of peculiar interest to study the interplay between chirality and magnetism, which are directly connected through magneto-chiral dichroism (M χ D), a phenomenon which arises from the coexistence of spatial asymmetry and magnetization in a material.^{47,48}

In this paper, we report on the synthesis and structural and magnetic characterization of two new octahedral Co^{II}-based helicates, obtained by using H₄L, cobalt(II) assembling cations,

and sodium carbonate to deprotonate the ligand.³³ For the molar ratio L⁴⁻:Co^{II} = 3:4, we obtained a 3-D coordination polymer, constructed from {Co^{II}₄} anionic helicates, connected by sodium ions: $\infty^3[\text{Co}_4\text{L}_3\text{Na}_4(\text{H}_2\text{O})_4]\cdot 4\text{H}_2\text{O}$ (1). By increasing the amount of cobalt(II) ions, namely to a 3:5 L⁴⁻:Co^{II} molar ratio, we succeeded in connecting the tetranuclear helicates through paramagnetic cobalt(II) ions, each cobalt ion replacing two sodium ions: $\infty^2[\text{Co}_5\text{L}_3\text{Na}_2(\text{H}_2\text{O})_9]\cdot 2.7\text{H}_2\text{O}\cdot \text{DMF}$ (2).

EXPERIMENTAL SECTION

Materials. Reactions were carried out under a normal atmosphere. The chemicals used were of reagent grade and were purchased from commercial sources. H₄L was prepared as previously described.³³

Syntheses. $\infty^3[\text{Co}_4\text{L}_3\text{Na}_4(\text{H}_2\text{O})_4]\cdot 4\text{H}_2\text{O}$ (1). An aqueous solution of Na₂CO₃·6H₂O (0.171 g, 0.6 mmol) was added to a stirred suspension of H₄L (0.098 g, 0.3 mmol) in DMF (10 mL). The resulting yellow solution was reacted with a solution of Co(ClO₄)₂·6H₂O (0.146 g, 0.4 mmol) in a minimum amount of DMF. An excess of sodium carbonate has been employed, in order to dissolve the helicand. The slow evaporation of a reddish orange reaction mixture, at room temperature, afforded red single crystals which were filtered, washed with ethanol, and allowed to dry in air. Yield: 75% based on H₄L. Anal. Calcd for C₄₈H₄₀Co₄N₆Na₄O₂₆: C, 39.91; H, 2.79; N, 5.82. Found: C, 40.73; H, 2.39; N, 6.75. IR data (KBr, cm⁻¹): 3434 (m), 1659 (m), 1600 (vs), 1549 (vs), 1457 (s), 1433 (s), 1378 (s), 1305 (m), 1226 (m), 879 (w), 764 (w), 660 (w). UV-vis-NIR diffuse reflectance spectrum (nm): 250 (sh), 450, 600 (sh), 1100 (Figure S1 in the Supporting Information).

$\infty^2[\text{Co}_5\text{L}_3\text{Na}_2(\text{H}_2\text{O})_9]\cdot 2.7\text{H}_2\text{O}\cdot \text{DMF}$ (2). An aqueous solution of Na₂CO₃·6H₂O (0.171 g, 0.6 mmol) was added to a stirred suspension of H₄L (0.098 g, 0.3 mmol) in a DMF/H₂O (2/1) mixture (10 mL). A yellow solution was formed and further reacted with a solution of Co(ClO₄)₂·6H₂O (0.183 g, 0.5 mmol) in a minimum amount of water. The slow evaporation of the resulting solution, at room temperature, afforded red single crystals which were isolated by filtration, washed with water (to remove the possible traces of water-soluble complex 1) and isopropyl alcohol, and allowed to air-dry. Yield: 70% based on H₄L. Anal. Calcd for C₅₁H_{54.4}Co₃N₇Na₂O_{30.7}: C, 38.35; H, 3.43; N, 6.14. Found: C,

38.81; H, 3.91; N, 6.31. IR data (KBr, cm^{-1}): 3363 (m), 1656 (m), 1600 (vs), 1548 (vs), 1455 (s), 1432 (s), 1378 (s), 1300 (m), 1225 (m), 879 (w), 763 (w), 661 (w). UV–vis–NIR diffuse reflectance spectrum (nm): 250 (sh), 460, 600 (sh), 1010 (Figure S1 in the Supporting Information). The number of crystallization solvent molecules has been confirmed by thermal analysis (Figure S2 in the Supporting Information).

Physical Measurements. The IR spectra of **1** and **2** were recorded on a FTIR Bruker Tensor V-37 spectrophotometer as KBr pellets in the 4000–400 cm^{-1} range at room temperature. The UV–vis–NIR spectra were recorded, in the solid state, with a V-670 Jasco spectrophotometer in the 2000–200 nm range. dc magnetic characterization of **1** and **2** was performed by using a MPMS Quantum Design SQUID magnetometer, applying a field of 1 kOe from 2 to 40 K and of 10 kOe from 30 to 300 K. Raw magnetic data were corrected for the sample holder and diamagnetic contributions to extract the paramagnetic molar magnetization as a function of field and temperature. The susceptibility is then evaluated as the ratio $\chi_M = M_M/H_{dc}$, where H_{dc} is the applied magnetic field. Dynamic magnetic data were collected by using the ac measurement system option of a PPMS Quantum Design setup.

Crystallographic Data Collection and Structure Determination. Details about data collection and solution refinement are given in Table 1. X-ray diffraction measurements were performed on a STOE IPDS II diffractometer operating with a Mo $K\alpha$ ($\lambda = 0.71073 \text{ \AA}$) X-ray tube with graphite monochromator for complex **1** and on an Xcalibur Eos diffractometer operating with a Mo $K\alpha$ ($\lambda = 0.71073 \text{ \AA}$) X-ray tube with graphite monochromator for complex **2**. The structures were solved by direct methods using SHELXS-97 and refined by full-matrix least squares on F^2 with SHELXL-97⁴⁹ with anisotropic displacement parameters for non-hydrogen atoms, except those with partial *sof*. All H atoms attached to carbon were introduced in idealized positions using the riding model with their isotropic displacement parameters fixed at 120% of the value for their riding atom. Positional parameters of the H atoms attached to coordinated water molecules were obtained from difference Fourier syntheses and verified by the geometric parameters of the corresponding hydrogen bonds. For compound **1** the structure has been refined as two component twin (twin law: $-100/010/00-1$) in space group $Abm2$. Crystallographic data for the structures have been deposited in the Cambridge Crystallographic Data Centre, deposition numbers CCDC 1557267 for **1** and CCDC 1557728 for **2**. These data can be obtained free of charge from the Cambridge Crystallographic Data Centre via www.ccdc.cam.ac.uk/data_request/cif. Powder X-ray diffraction (PXRD) measurements were carried out on a Bruker D8 Discover instrument (Cu $K\alpha 1$ radiation, $\lambda \approx 1.5418 \text{ \AA}$) equipped with a Lynxeye 1D detector in parallel beam geometry. The samples were mounted on a quartz low-background sample holder and scanned in the range $5-50^\circ$ (2θ) with a step size of 0.04° (2θ) and a dwell time of 1 s/step.

RESULTS AND DISCUSSION

Description of Structures. The crystal structures of the two compounds have been solved. Since the two compounds have been obtained from the same starting materials, we checked their purity by PXRD. The two diffractograms, compared with the simulated measurements (Figures S3 and S4 in the Supporting Information), confirm the purity of the crystalline phases.

Let us discuss briefly the structure of **1**. It consists of tetranuclear triple-stranded tetraanionic helicates (Figure 1), connected through sodium ions. Within each anionic entity the three ligands are twisted along the central N–N single bonds, resulting in four compartments hosting the cobalt(II) ions. The peripheral cobalt ions (Co1, Co1ⁱ, $i = -2 - x, -y, z$) are coordinated by three carboxylato and three phenoxido oxygen atoms (bond lengths varying between 2.037(10) and 2.120(10) \AA), with a distorted-trigonal-prismatic geometry. The inner cobalt ions (Co2, Co2ⁱ, $i = -2 - x, -y, z$) are coordinated by three phenoxido oxygens (2.050(10)–2.083(10) \AA) and by three nitrogen atoms (2.109(12)–2.135(12) \AA), with a

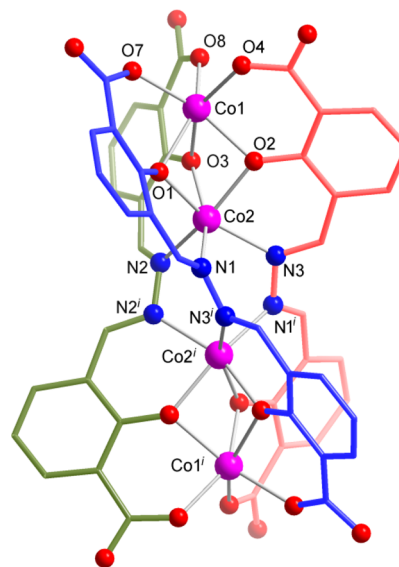


Figure 1. View of the tetranuclear triple-stranded tetraanionic helicate in **1**. Symmetry codes: $i = -2 - x, -y, z$.

distorted-octahedral geometry. The distances between the cobalt ions are $\text{Co1}\cdots\text{Co2} = 2.929 \text{ \AA}$ and $\text{Co2}\cdots\text{Co2}^i = 3.586 \text{ \AA}$. The sodium ions are bridged by the carboxylato oxygen atoms and by water molecules (Figure S5 in the Supporting Information), forming layers paralleling the *ac* plane. The 3-D architecture of the crystal can be described as being formed by parallel layers made by sodium ions, connected by $\{\text{Co}_4\}$ pillars of opposite chiralities (Figure 2).

Compound **2** illustrates that the anionic helicates can be connected by paramagnetic metal ions as well, resulting in coordination polymers, which are expected to show magnetic properties more complex than those of the isolated helicates. The triple-stranded helicate unit is similar to that observed in crystal **1**, but in this case the four cobalt ions are crystallographically independent (Figure 3). The fifth cobalt ion (Co5) connects two helicates, interacting with the oxygen atoms from two carboxylate groups belonging to two helicates with opposite chiralities (Figure 4), resulting in infinite chains. The distances between the cobalt ions are as follows: $\text{Co1}\cdots\text{Co2} = 2.918 \text{ \AA}$, $\text{Co2}\cdots\text{Co3} = 3.601 \text{ \AA}$, $\text{Co3}\cdots\text{Co4} = 2.887 \text{ \AA}$, $\text{Co4}\cdots\text{Co5} = 3.876 \text{ \AA}$, $\text{Co5}\cdots\text{Co1}^i = 5.348 \text{ \AA}$ ($i = 0.5 + x, 0.5 - y, -0.5 + z$). The Co5 ion shows a distorted-octahedral geometry: it is coordinated by one carboxylato oxygen from a group bridging Co5 to Co1 (syn-anti bridging mode), by a chelating carboxylate group that connects Co5 to Co1ⁱ (monatomic bridging), and by three aqua ligands (two of them make a double bridge between Co5 and Na1). These chains are then connected by the chains made by the sodium ions. Layers running along the crystallographic *b* axes are thus formed (Figure 5). None of the two crystallographically independent sodium ions interact directly with the oxygen atoms of the helicates. They are bridged solely by aqua ligands. The Na1 ions are also doubly bridged by aqua ligands to the Co5 ions (Figure S6 in the Supporting Information). Selected bond distances and angles for compounds **1** and **2** are collected in Table S1 in the Supporting Information.

Magnetic Properties. Static Magnetic Properties. The room-temperature value of the $\chi_M T$ product for compound **1** ($9.2 \text{ cm}^3 \text{ mol}^{-1} \text{ K}$) falls at the lower end of the expected range for four noncorrelated cobalt(II) ions, characterized by a non-negligible unquenched angular momentum: this suggests a

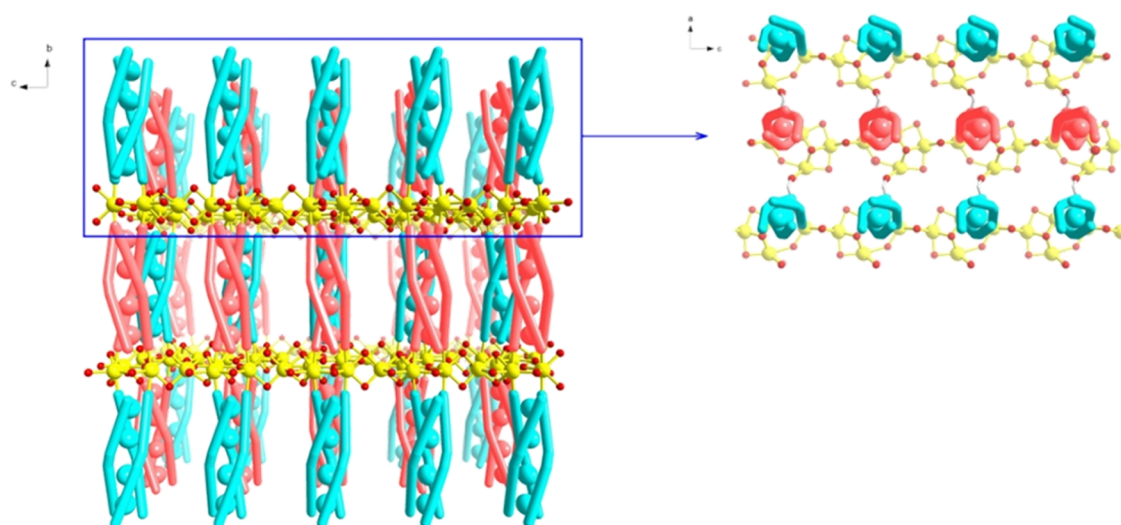


Figure 2. (left) Crystal packing of **1**, viewed along the *a* crystallographic axis. (right) Representation of a layer constructed of $[\text{Co}_4\text{L}_3]^{4+}$ helicates, superimposed over a layer of sodium(I) ions, along the *b* crystallographic axis. Color codes: cyan, *P* helicity; red, *M* helicity.

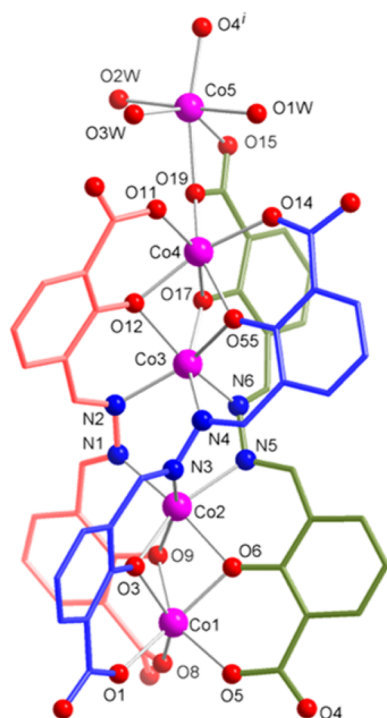


Figure 3. (a) View of $\{\text{Co}_3\}$ repeating unit in **2**. Symmetry codes: $i = 0.5 + x, 0.5 - y, -0.5 + z$.

relatively large distortion from purely octahedral geometry.⁵⁰ On lowering the temperature (see Figure 6 and Figure S6 in the Supporting Information) $\chi_M T$ decreases gradually until 150 K and then more markedly, to reach $0.36 \text{ cm}^3 \text{ mol}^{-1} \text{ K}$ at 1.8 K. While the high-temperature decrease can be traced back to progressive depopulation of the excited doublets arising from the combined effect of low-symmetry distortions and spin–orbit coupling on the $^4\text{T}_{1g}$ state of octahedral Co^{II} , the low-temperature decrease strongly hints at the presence of antiferromagnetic exchange coupling interactions mediated by the phenoxido and diazine bridges. Since the ground state for four linearly arranged antiferromagnetically coupled Co^{II} ions is diamagnetic, the nonzero value of the $\chi_M T$ product at 1.8 K can be attributed to the presence of a paramagnetic impurity, which is

indeed clearly evidenced by both the χ_M vs *T* curve and the isothermal *M* vs *H* curve measured at low temperature (Figures S7–S9 in the Supporting Information). The latter could be fit by assuming a Brillouin contribution for a species with an effective $S_{\text{eff}} = 1/2$ (due to the impurity) and the temperature-independent paramagnetism contribution due to the four Co^{II} centers of the cluster, which accounts for the high-field linear increase of the isothermal magnetization curves. The best-fit parameters provided $g_{\text{iso}}(\text{impurity}) = 4.29 \pm 0.07\%_{\text{IMP}} = 0.136 \pm 0.002$ and $\chi_{\text{TIP}} = (5.3 \pm 0.6) \times 10^{-2} \text{ cm}^3 \text{ mol}^{-1}$. These parameters strongly suggest that the paramagnetic impurity is due to a monomeric Co^{II} -containing species, possibly due to some cluster fragmentation occurring during the synthetic procedure. The estimated contribution of the paramagnetic impurity was then subtracted from both the *M* vs *H* curve and the temperature dependence of the susceptibility (corrected data are reported in Figure 6) before attempting a fit of the data.

A quantitative analysis of the observed magnetic behavior is nonetheless far from trivial in this case. We have in principle to consider two structurally different cobalt centers, for each of which at least three single-ion parameters have to be defined (spin–orbit coupling, axial distortion, orbital reduction factor). Further, two different exchange coupling constants are expected, across phenoxido and diazine bridges, respectively. This makes a total of eight parameters at least and, further, a dimension of the problem which is computationally expensive, as we have to consider both spin and orbital degrees of freedom ($12^4 \times 12^4$). Finally, the literature on magnetostructural correlations for Co^{II} exchange coupled systems is extremely scarce, due to the ease of parametrization and complexity of the treatment required for a quantitative analysis of magnetic data of Co^{II} centers. However, the few reports on systems showing structural features similar to those of **1** consistently point to weak antiferromagnetic interactions mediated by both triple diazine^{33,51,52} and phenoxido bridges.^{53,54}

To reduce the overparametrization of the problem, we then considered a common set of single-ion parameters for the two crystallographically independent cobalt(II) centers and further assumed the diazine transmitted coupling to be negligible: this amounts to consideration of the system as the sum of two antiferromagnetically coupled dimers with no intradimer

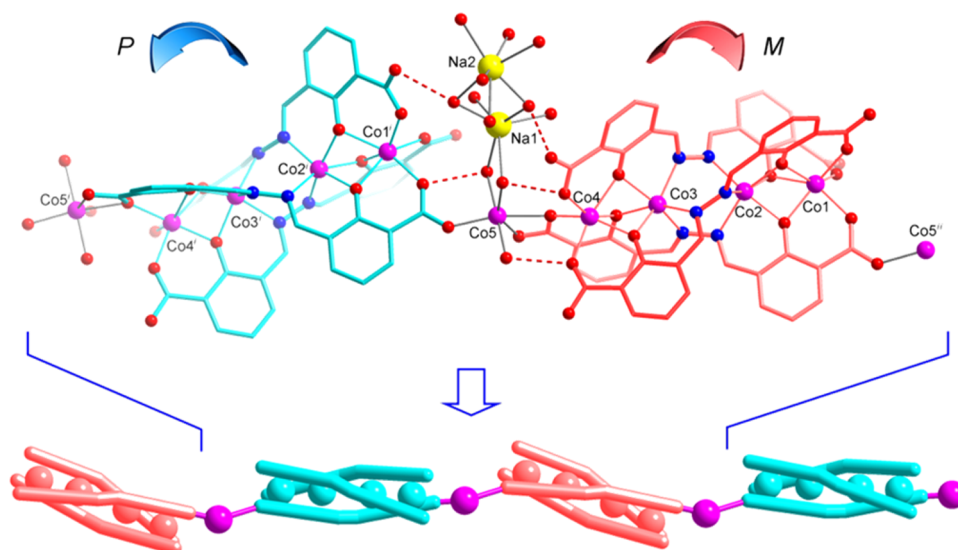


Figure 4. Perspective view of the chains resulting from connecting $\{\text{Co}_4\}$ anionic helicates by cobalt(II) ions in **2**. Color codes: cyan, *P* helicity; red, *M* helicity. Symmetry codes: i = $-0.5 + x, 0.5 - y, 0.5 + z$; ii = $0.5 + x, 0.5 - y, -0.5 + z$.

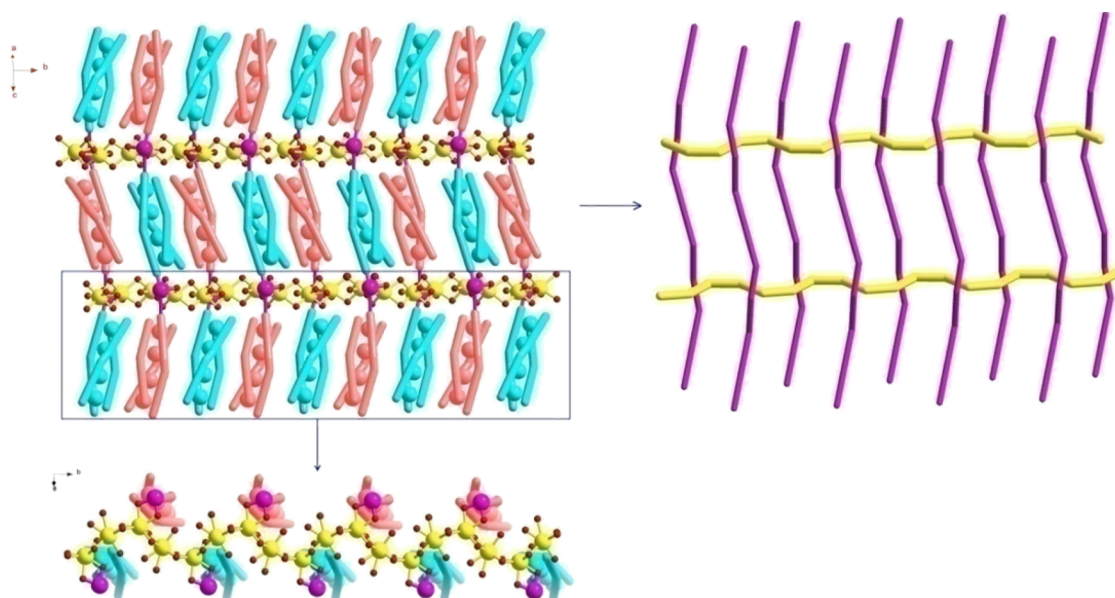


Figure 5. Crystal packing of **2**, viewed from two different directions. Color codes: cyan, *P* helicity; red, *M* helicity (left). Schematic view of the $\{\text{Co}_3\}_n$ chains (purple) and of the chains constructed from sodium ions (yellow) -right.

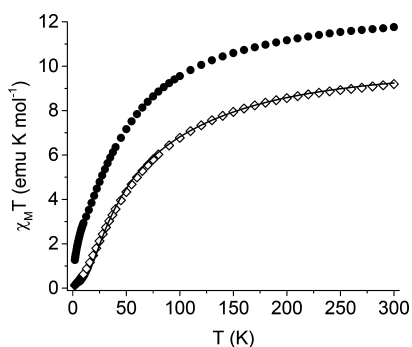


Figure 6. $\chi_M T$ vs T plot for **1** (empty squares) and **2** (full circles). Data of **1** have been corrected for the paramagnetic impurity present in the sample (see text for details). The continuous line is the best fit to the data using the dimer model and parameters reported in the text.

interaction. While this is clearly a simplification, it should provide an upper bound on the exchange coupling transmitted by the phenoxido bridges. The Hamiltonian employed for fitting the data⁵⁵ was then

$$\hat{H} = \beta H [g_e \sum_{i=1}^2 \hat{S}_i - \alpha \sum_{i=1}^2 \hat{S}'_i] + \Delta \sum_{i=1}^2 (\hat{S}'_i z^2 - 2/3) - \alpha \lambda \sum_{i=1}^2 \hat{S}_i \hat{S}'_i - 2J \hat{S}_1 \hat{S}_2 \quad (1)$$

where $S_i = 3/2$ is the spin of Co^{II} ions, $S'_i = 1$ is the fictitious spin by which the orbital angular momentum $L = 1$ of the $^4\text{T}_{1g}$ state of Co^{II} is modeled, α takes into account both the orbital reduction factor due to covalency and the T–P isomorphism, λ is the multielectron spin–orbit coupling constant, Δ the axial distortion parameter, and J is the isotropic exchange coupling

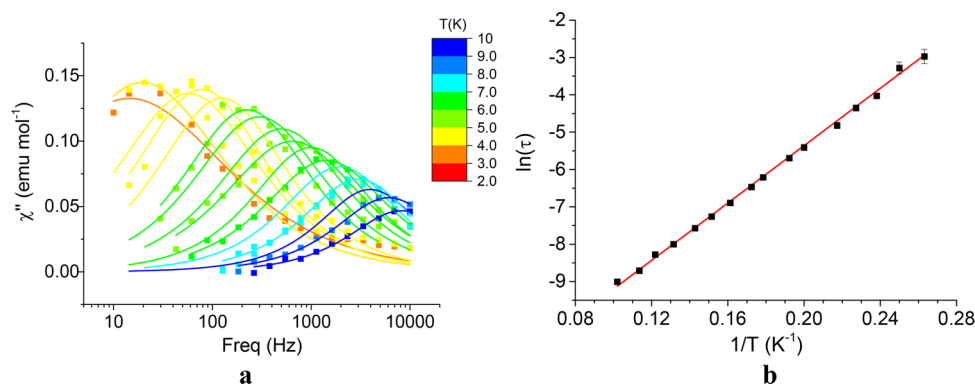


Figure 7. (a) Temperature dependence of $\chi''(\nu)$ of **2** and best fit to Debye equation. (b) Corresponding Arrhenius plot using τ values extracted by a Debye fit of the $\chi''(\nu)$ curves and best linear fit with parameters reported in the text.

constant between the isotropic $S = 3/2$ spins.⁵⁰ This provided as a best fit the following parameters: $\Delta = -110 \pm 10 \text{ cm}^{-1}$, $\lambda = -230 \pm 20 \text{ cm}^{-1}$, $\alpha = 1.04 \pm 0.02$, and $J = -4.60 \pm 0.03 \text{ cm}^{-1}$. It is worth noting that Δ , λ , and α values are greatly correlated and the obtained values should then be considered with much caution. At any rate, the obtained picture points to a ground pseudodoublet, split by about 2.0 cm^{-1} , with a first excited doublet ca. 40 cm^{-1} above it (see Table S2 in the Supporting Information). The obtained value for the phenoxido-transmitted coupling is quite close to those reported by Aromi and co-workers for structurally similar systems, thus lending some support to the obtained values.⁵⁶

The temperature dependence of the $\chi_M T$ product for compound **2** is also shown in Figure 6. Even in this case the room-temperature value ($11.8 \text{ cm}^3 \text{ mol}^{-1} \text{ K}$) falls at the lower end of the expected range for five uncorrelated Co^{II} ions. Upon cooling, $\chi_M T$ decreases gradually to 150 K and then more abruptly, to reach $1.3 \text{ cm}^3 \text{ mol}^{-1} \text{ K}$ at 1.8 K . The nonzero value at low temperature is consistent with the odd number of Kramers ions per molecule, which can only give rise to a magnetic ground state, even in the presence of antiferromagnetic interactions. This is further confirmed by the M vs H curve, which is consistent with expectation for a single Co^{II} center at low temperature. This behavior can be qualitatively explained by considering the strict similarity of the structures of the magnetic cores of **1** and **2**, which is only broken by the extra Co^{II} ion (Co5) in the latter. At low temperature, the Co_4 subunit of **2** is expected, on the basis of the results of **1**, to be in a diamagnetic ground state. If the interaction of Co5 with the Co_4 unit, mediated by the syn-anti carboxylato bridge, is weaker than those mediated by diazine and phenoxido bridges, the low-temperature magnetic properties of **2** are expected to be essentially determined by those of the Co5 center. In this respect it is however worth noting that the carboxylato bridge is expected to transmit a ferromagnetic interaction of magnitude comparable to the antiferromagnetic ones observed in the Co_4 unit, thus making a simple analysis based on the properties of Co5 only, unfeasible.⁵⁷

Dynamic Magnetic Properties. Dynamic magnetic susceptibility was measured for both samples in zero and applied field (Figure 7 and Figures S10 and S11 in the Supporting Information). While no χ'' signal was observed for **1**, as expected on the basis of the diamagnetic nature of its ground state, a clear frequency-dependent signal was observed for **2**. No relevant field dependence could be observed for the dynamic behavior of **2** at 2 K (Figure S10). These observations may be traced back to the fact that the observed dynamic behavior is due to the single,

uncorrelated Co5 center, which is already quite well diluted in an essentially diamagnetic matrix of Co_4 moieties. This makes dipolar-induced relaxation in zero field (i.e., quantum tunneling type processes) very inefficient, allowing the observation of dynamic behavior even in zero field (Figure S11). At the same time, the constancy of the observed rate with field suggests that the direct process is not playing a relevant role in the relaxation. The fit of the frequency dependence of the ac susceptibility measured at variable temperatures using the Debye equation⁵⁸ allowed us to derive the thermal dependence of the relaxation rate and its distribution, α , which decreases from 0.3 at 3.6 K to 0.05 at 9.8 K . This provided a linear Arrhenius plot, as expected for a thermally activated Orbach process (Figure 7b). The fit afforded an effective energy barrier for the reversal of the magnetization, $\Delta E_{\text{eff}}/k = 38.4 \pm 0.5 \text{ K}$ ($\Delta E_{\text{eff}} = 26.7 \pm 0.3 \text{ cm}^{-1}$) with $\tau_0 = (2.3 \pm 0.2) \times 10^{-6} \text{ s}$. We note here that the obtained value for the effective barrier might not reflect the actual existence of a real state at that energy,⁵⁹ since it is much lower than expected for a Co^{II} center. This is a point often reported for octahedral Co^{II} -based complexes^{60–62} and prompted us to look for the possible presence of other relaxation by including a dominant Raman term, in combination with Orbach or quantum tunneling processes (despite the fact that field-dependent dynamics would tend to exclude this). None of these provided fits as good as the Orbach fit (Figure S12 in the Supporting Information), which is then favored by this analysis. The apparent discrepancy, often reported for single-molecule magnets, between the experimentally determined activation energy and the energy of the first excited state has been recently theoretically explained for a model $S = 1$ system by considering the role of anharmonic phonons. In particular, it was shown that “the finite line width of the phonons spectral distribution allows an Orbach-type spin relaxation mechanism even when the phonon is not resonant at the spin excitation”.⁶³ While further spectroscopic and theoretical investigation would be necessary to confirm the exact mechanism by which slow relaxation occurs in **2**, it is tempting to assign the observation of a linear Arrhenius plot with ΔE_{eff} largely different from the energy of the $1s$ excited state to such a phenomenon.

CONCLUSIONS

In conclusion, we have shown that anionic helicates with potentially bridging groups can be employed as building blocks in constructing heterometallic coordination polymers. The two compounds described herein have been obtained from the same starting materials, but with different Co^{II} :helicand molar ratios.

An excess of cobalt(II) ions leads to chains constructed from $\{\text{Co}^{\text{II}}_4\}$ helicates and single Co^{II} ions, the helicate acting as a metalloligand toward both sodium and cobalt ions. This interesting topology of $[\{\text{Co}^{\text{II}}_4\}\text{Co}]_n$ allowed us to emphasize the slow relaxation of the magnetization for the single Co^{II} ions, which, at low temperatures, are the sole paramagnetic centers, the tetranuclear helicates being characterized by a diamagnetic ground state. The relaxation process apparently follows Orbach's mechanism even if conclusive proof about the actual relaxation process would require a detailed spectroscopic and theoretical investigation of the system, which is beyond the scope of this paper. This chemistry can be expanded using other paramagnetic assembling cations. Further work on such systems is in progress in our laboratories.

■ ASSOCIATED CONTENT

● Supporting Information

The Supporting Information is available free of charge on the ACS Publications website at DOI: [10.1021/acs.inorgchem.7b01640](https://doi.org/10.1021/acs.inorgchem.7b01640).

Diffuse reflectance spectra, selected bond distances and angles, thermal analysis, PXRD data, packing diagrams, molar magnetic susceptibility vs temperature data, magnetization vs field data, and energy levels (PDF)

Accession Codes

CCDC 1557267 and 1557728 contain the supplementary crystallographic data for this paper. These data can be obtained free of charge via www.ccdc.cam.ac.uk/data_request/cif, or by emailing data_request@ccdc.cam.ac.uk, or by contacting The Cambridge Crystallographic Data Centre, 12 Union Road, Cambridge CB2 1EZ, UK; fax: +44 1223 336033.

■ AUTHOR INFORMATION

Corresponding Authors

*E-mail for L.S.: lorenzo.sorace@unifi.it.

*E-mail for M.A.: marius.andruh@dnt.ro.

ORCID

Lorenzo Sorace: 0000-0003-4785-1331

Marius Andruh: 0000-0001-8224-4866

Notes

The authors declare no competing financial interest.

■ ACKNOWLEDGMENTS

The financial support of the Italian and Romanian foreign affair secretariat through the project Multifunctional Molecular Nanosystems is gratefully acknowledged.

■ REFERENCES

- (1) Constable, E. C. *Metallosupramolecular chemistry*. *Chem. Ind.* **1994**, 56–59.
- (2) *Comprehensive Supramolecular Chemistry*; Constable, E. C., Lehn, J.-M., Atwood, L., Davis, J. E. D., MacNicol, D. D., Vögtle, F., Eds.; Pergamon: Oxford, U.K., 1996; Vol. 9, p 213.
- (3) Leininger, S.; Olenyuk, B.; Stang, P. J. Self-assembly of discrete cyclic nanostructures mediated by transition metals. *Chem. Rev.* **2000**, *100*, 853–908.
- (4) Holliday, B. J.; Mirkin, C. A. Strategies for the Construction of supramolecular compounds through coordination chemistry. *Angew. Chem., Int. Ed.* **2001**, *40*, 2022–2043.
- (5) Lehn, J.-M. *Supramolecular Chemistry-Concepts and Perspectives*; VCH: Weinheim, Germany, 1995; pp 1–281.

- (6) Piguet, C.; Bernardinelli, G.; Hopfgartner, G. Helicates as versatile supramolecular complexes. *Chem. Rev.* **1997**, *97*, 2005–2062.
- (7) Albrecht, M. Dicatechol ligands: novel building-blocks for metallosupramolecular chemistry. *Chem. Soc. Rev.* **1998**, *27*, 281–288.
- (8) Albrecht, M. "Let's twist again" - Double-stranded, triple-stranded, and circular helicates. *Chem. Rev.* **2001**, *101*, 3457–3497.
- (9) Hannon, M. J.; Childs, L. J. Helices and helicates: beautiful supramolecular motifs with emerging applications. *Supramol. Chem.* **2004**, *16*, 7–22.
- (10) Piguet, C.; Borkovec, M.; Hamacek, J.; Zeckert, K. Strict self-assembly of polymetallic helicates: the concepts behind the semantics. *Coord. Chem. Rev.* **2005**, *249*, 705–726.
- (11) Lehn, J.-M. Programmed chemical systems: multiple subprograms and multiple processing/expression of molecular information. *Chem. - Eur. J.* **2000**, *6*, 2097–2102.
- (12) Lehn, J.-M. Toward self-organization and complex matter. *Science* **2002**, *295*, 2400–2403.
- (13) Habib, F.; Murugesu, M. Lessons learned from dinuclear lanthanide nano-magnets. *Chem. Soc. Rev.* **2013**, *42*, 3278–3288.
- (14) Woodruff, D. N.; Wimpenny, R. E. P.; Layfield, R. A. Lanthanide single-molecule magnets. *Chem. Rev.* **2013**, *113*, 5110–5148.
- (15) Cucos, P.; Tuna, F.; Sorace, L.; Matei, I.; Maxim, C.; Shova, S.; Gheorghe, R.; Caneschi, A.; Hillebrand, M.; Andruh, M. Magnetic and luminescent binuclear double-stranded helicates. *Inorg. Chem.* **2014**, *53*, 7738–7747.
- (16) Floquet, S.; Ouali, N.; Bocquet, B.; Bernardinelli, G.; Imbert, D.; Bünzli, J. C. G.; Hopfgartner, G.; Piguet, C. The first self-assembled trimetallic lanthanide helicates driven by positive cooperativity. *Chem. - Eur. J.* **2003**, *9*, 1860–1875.
- (17) Albrecht, M. Homodinuclear *f-f* and heterodinuclear *f-p* lanthanide helicates. *Z. Anorg. Allg. Chem.* **2010**, *636*, 2198–2204.
- (18) Albrecht, M.; Osetska, O.; Bünzli, J. C. G.; Gumy, F.; Fröhlich, R. Homo- and heterodinuclear helicates of Lanthanide(III), Zinc(II) and Aluminium(III) based on 8-hydroxyquinoline ligands. *Chem. - Eur. J.* **2009**, *15*, 8791–8799.
- (19) Vandevyver, C. D. B.; Chauvin, A.-S.; Comby, S.; Bünzli, J. C. G. Luminescent lanthanide bimetallic triple-stranded helicates as potential cellular imaging probes. *Chem. Commun.* **2007**, 1716–1718.
- (20) Fernández-Moreira, V.; Song, B.; Sivagnanam, V.; Chauvin, A.-S.; Vandevyver, C. D. B.; Gijjs, M.; Hemmilä, I.; Lehr, H.-A.; Bünzli, J. C. G. Bioconjugated lanthanide luminescent helicates as multilabels for lab-on-a-chip detection of cancer biomarkers. *Analyst* **2010**, *135*, 42–52.
- (21) Chauvin, A.-S.; Comby, S.; Baud, M.; De Piano, C.; Duhot, C.; Bünzli, J. C. G. Luminescent lanthanide helicates self-assembled from ditopic ligands bearing phosphonic acid or phosphoester units. *Inorg. Chem.* **2009**, *48*, 10687–10696.
- (22) Elhabiri, M.; Scopelliti, R.; Bünzli, J. C. G.; Piguet, C. Lanthanide helicates self-assembled in water: A new class of highly stable and luminescent dimetallic carboxylates. *J. Am. Chem. Soc.* **1999**, *121*, 10747–10762.
- (23) Stomeo, F.; Lincheneau, C.; Leonard, J. P.; O'Brien, J. E.; Peacock, R. D.; McCoy, C. P.; Gunlaugsson, T. Metal-directed synthesis of enantiomerically pure dimetallic lanthanide luminescent triple-stranded helicates. *J. Am. Chem. Soc.* **2009**, *131*, 9636–9637.
- (24) Eliseeva, S. V.; Auböck, G.; van Mourik, F.; Cannizzo, A.; Song, B.; Deiters, E.; Chauvin, A.-S.; Chergui, M.; Bünzli, J. C. G. Multiphoton-excited luminescent lanthanide bioprobes: two- and three-photon cross sections of dipicolinate derivatives and binuclear helicates. *J. Phys. Chem. B* **2010**, *114*, 2932.
- (25) Leong, W. L.; Vittal, J. J. One-dimensional coordination polymers: complexity and diversity in structures, properties, and applications. *Chem. Rev.* **2011**, *111*, 688–764 and references therein.
- (26) Zhan, S.-Z.; Li, M.; Hou, J.-Z.; Ni, J.; Li, D.; Huang, X.-C. Polymerizing cluster helicates into high-connectivity networks. *Chem. - Eur. J.* **2008**, *14*, 8916–8921.
- (27) Sun, Q.; Wei, M.; Bai, Y.; He, C.; Meng, Q.; Duan, C. Entanglement of individual coordination polymers having helicates as building intermediates. *Dalton Trans.* **2007**, 4089–4094.

- (28) Yoo, H.; Lee, J.; Kang, P.; Choi, M.-G. Synthesis of cobalt cluster-based supramolecular triple-stranded helicates. *Dalton Trans.* **2015**, *44*, 14213–14216.
- (29) Hamblin, J.; Jackson, A.; Alcock, N. W.; Hannon, M. J. Triple helicates and planar dimers arising from silver(I) coordination to directly linked bis-pyridylimine ligands. *J. Chem. Soc., Dalton Trans.* **2002**, 1635–1641.
- (30) Hong, M.; Cheng-jie, F.; Chun-ying, D.; Yu-ting, L.; Qing-jin, M. Crystal structures of metal–organic frameworks sustained by π – π interactions between triple-helices. *Dalton Trans.* **2003**, 1229–1234.
- (31) Albrecht, M.; Janser, I.; Kamptmann, S.; Weis, P.; Wibbeling, B.; Fröhlich, R. Dicatechol-diimines: easily accessible ligands for the self-assembly of dinuclear triple-stranded helicates. *Dalton Trans.* **2004**, 37–43.
- (32) Sreerama, S. G.; Pal, S. Dinuclear triple helicates with diazine ligands: X-ray structural, electrochemical, and magnetic studies. *Inorg. Chem.* **2005**, *44*, 6299–6307.
- (33) Cucos, P.; Pascu, M.; Sessoli, R.; Avarvari, N.; Pontillart, F.; Andruh, M. Heterotopic helicand for designing heterometallic helicates. *Inorg. Chem.* **2006**, *45*, 7035–7037.
- (34) Gatteschi, D.; Vindigni, A. *Molecular Magnets*; Bartolomé, J., Luis, F., Fernandez, J. F., Eds.; Springer-Verlag: Berlin, Heidelberg, 2014.
- (35) Frost, J. M.; Harriman, K. L. M.; Murugesu, M. The rise of 3-*d* single-ion magnets in molecular magnetism: towards materials from molecules? *Chem. Sci.* **2016**, *7*, 2470–2491.
- (36) Bar, A. K.; Pichon, C.; Sutter, J.-P. Magnetic anisotropy in two- to eight-coordinated transition–metal complexes: Recent developments in molecular magnetism. *Coord. Chem. Rev.* **2016**, *308*, 346–380.
- (37) Gómez-Coca, S.; Urtizberea, A.; Cremades, E.; Alonso, P. J.; Camón, A.; Ruiz, E.; Luis, F. Origin of slow magnetic relaxation in Kramers' ions with non-uniaxial anisotropy. *Nat. Commun.* **2014**, *5*, 4300.
- (38) Vallejo, J.; Castro, I.; Ruiz-García, R.; Cano, J.; Julve, M.; Lloret, F.; De Munno, G.; Wernsdorfer, W.; Pardo, E. Field-induced slow magnetic relaxation in a six-coordinate mononuclear cobalt(II) complex with a positive anisotropy. *J. Am. Chem. Soc.* **2012**, *134*, 15704–15707.
- (39) Colacio, E.; Ruiz, J.; Ruiz, E.; Cremades, E.; Krzystek, J.; Carretta, S.; Cano, J.; Guidi, T.; Wernsdorfer, W.; Brechin, E. K. Slow magnetic relaxation in a $\text{Co}^{\text{II}}\text{-Y}^{\text{III}}$ single-ion magnet with positive axial zero-field splitting. *Angew. Chem., Int. Ed.* **2013**, *52*, 9130–9134.
- (40) Zhu, Y. Y.; Cui, C.; Zhang, Y. Q.; Jia, J. H.; Guo, X.; Gao, C.; Qian, K.; Jiang, S. D.; Wang, B. W.; Wang, Z. M.; Gao, S. Zero-field slow magnetic relaxation from single Co(II) ion: a transition metal single-molecule magnet with high anisotropy barrier. *Chem. Sci.* **2013**, *4*, 1802–1806.
- (41) Pali, A. V.; Korchagin, D. V.; Yureva, E. A.; Akimov, A. V.; Misochko, E. Y.; Shilov, G. V.; Talantsev, A. D.; Morgunov, R. B.; Aldoshin, S. M.; Tsukerblat, B. S. Single-ion magnet $\text{Et}_2\text{N}[\text{Co}^{\text{II}}(\text{hfac})_3]$ with nonuniaxial anisotropy: synthesis, experimental characterization, and theoretical modeling. *Inorg. Chem.* **2016**, *55*, 9696–9706.
- (42) Herchel, R.; Váhovská, L.; Potočňák, I.; Trávníček, Z. Slow magnetic relaxation in octahedral cobalt(II) field-induced single-ion magnet with positive axial and large rhombic anisotropy. *Inorg. Chem.* **2014**, *53*, 5896–5898.
- (43) Walsh, J. P. S.; Bowling, G.; Ariciu, A.-M.; Jailani, N. F. M.; Chilton, N. F.; Waddell, P. G.; Collison, D.; Tuna, F.; Higham, L. J. Evidence of slow magnetic relaxation in $\text{Co}(\text{AcO})_2(\text{py})_2(\text{H}_2\text{O})_2$. *Magnetochemistry* **2016**, *2*, 23–33.
- (44) Świtlicka-Olszewska, A.; Palion-Gazda, J.; Klemens, T.; Machura, B.; Vallejo, J.; Cano, J.; Lloret, F.; Julve, M. Single-ion magnet behaviour in mononuclear and two-dimensional dicyanamide-containing cobalt(II) complexes. *Dalton Trans.* **2016**, *45*, 10181–10193.
- (45) Buvaylo, E. A.; Kokozay, V. N.; Vassilyeva, O.; Yu; Skelton, B. W.; Ozarowski, A.; Titiš, J.; Vranovičová, B.; Boča, R. Field-assisted slow magnetic relaxation in a six-coordinate Co(II)–Co(III) complex with large negative anisotropy. *Inorg. Chem.* **2017**, *56*, 6999–7009.
- (46) Goswami, S.; Leitus, G.; Tripuramallu, B. K.; Goldberg, I. Mn^{II} and Co^{II} coordination polymers showing field-dependent magnetism and slow magnetic relaxation behavior. *Cryst. Growth Des.* **2017**, *17*, 4393–4404.
- (47) Train, C.; Gheorghe, R.; Krstic, V.; Chamoreau, L.-M.; Ovanesyana, N. S.; Rikken, G. L. J. A.; Gruselle, M.; Verdager, M. Strong magneto-chiral dichroism in enantiopure chiral ferromagnets. *Nat. Mater.* **2008**, *7*, 729–734.
- (48) Sessoli, R.; Boulon, M.-E.; Caneschi, A.; Mannini, M.; Poggini, L.; Wilhelm, F.; Rogalev, A. Strong magneto-chiral dichroism in a paramagnetic molecular helix observed by hard X-rays. *Nat. Phys.* **2014**, *11*, 69–74.
- (49) Sheldrick, G. M. *SHELXL-97: Programs for the Refinement of Crystal Structures*; University of Göttingen, Göttingen, Germany, 1996.
- (50) Lloret, F.; Julve, M.; Cano, J.; Ruiz-García, R.; Pardo, E. Magnetic properties of six-coordinated high-spin cobalt(II) complexes: Theoretical background and its application. *Inorg. Chim. Acta* **2008**, *361*, 3432–3445.
- (51) Wang, N.; Feng, Y.-C.; Shi, W.; Zhao, B.; Cheng, P.; Liao, D.-Z.; Yan, S.-P. Synthesis, structure, fluorescent and magnetic properties of a series of coordination polymers based on a long and flexible bis-triazole ligand. *CrystEngComm* **2012**, *14*, 2769–2778.
- (52) Sharga, O. V.; Lysenko, A. B.; Handke, M.; Krautscheid, H.; Rusanov, E. B.; Chernega, A. N.; Krämer, K. W.; Liu, S.-X.; Decurtins, S.; Bridgeman, A.; Domasevitch, K. V. Unprecedented trapping of difluoroctamolybdate anions within an α -Polonium type coordination network. *Inorg. Chem.* **2013**, *52*, 8784–8794.
- (53) Barrios, L. A.; Borilovic, I.; Uber, J. S.; Aguilà, D.; Roubeau, O.; Aromí, G. A new type of paddle-wheel coordination complex. *Dalton Trans.* **2013**, *42*, 12185–12192.
- (54) Aromí, G.; Evans, H. S.; Teat, S. J.; Cano, J.; Ribas, J. Di- and trinuclear Co^{II} complexes of a bis- β -diketone ligand with variable conformation: structure and magnetic studies. *J. Mater. Chem.* **2006**, *16*, 2635–2644.
- (55) Chilton, N. F.; Anderson, R. P.; Turner, L. D.; Soncini, A.; Murray, K. S. PHI: A powerful new program for the analysis of anisotropic monomeric and exchange-coupled polynuclear *d*- and *f*-block complexes. *J. Comput. Chem.* **2013**, *34*, 1164–1175.
- (56) Karmakar, T. K.; Aromí, G.; Ghosh, B. K.; Usman, A.; Fun, H. K.; Mallah, T.; Behrens, U.; Solans, X.; Chandra, S. K. Unexpected diversity and novel features within a family of new azide-bridged Mn(II) complexes of pyridyl/imine ligand. *J. Mater. Chem.* **2006**, *16*, 278–285.
- (57) Zhang, C.; Liu, Z.-Y.; Liu, N.; Zhao, H.; Yang, E. C.; Zhao, X. J. Different magnetic responses observed in Co, Co and Co-based MOFs. *Dalton Trans.* **2016**, *45*, 11864–11875.
- (58) Gatteschi, D.; Sessoli, R.; Villain, J. *Molecular nanomagnets*; Oxford University Press: Oxford, U.K., 2006.
- (59) Lucaccini, E.; Sorace, L.; Perfetti, M.; Costes, J.-P.; Sessoli, R. Beyond the anisotropy barrier: slow relaxation of the magnetization in both easy-axis and easy-plane Ln(trensal) complexes. *Chem. Commun.* **2014**, *50*, 1648–1651.
- (60) Zhang, Y.-Z.; Gómez-Coca, S.; Brown, A. J.; Saber, M. R.; Zhang, X.; Dunbar, K. R. Trigonal antiprismatic Co(II) single molecule magnets with large uniaxial anisotropies: importance of Raman and tunneling mechanisms. *Chem. Sci.* **2016**, *7*, 6519–6527.
- (61) Roy, S.; Oyarzabal, I.; Vallejo, J.; Cano, J.; Colacio, E.; Bauza, A.; Frontera, A.; Kirillov, A. M.; Drew, M. G. B.; Das, S. Two polymorphic forms of a six-coordinate mononuclear cobalt(II) complex with easy-plane anisotropy: structural features, theoretical calculations, and field-induced slow relaxation of the magnetization. *Inorg. Chem.* **2016**, *55*, 8502–8513.
- (62) Chandrasekhar, V.; Dey, A.; Mota, A. J.; Colacio, E. Slow magnetic relaxation in Co(III)–Co(II) mixed-valence dinuclear complexes with a $\text{Co}^{\text{II}}\text{O}_3\text{X}$ ($\text{X} = \text{Cl}, \text{Br}, \text{NO}_3$) distorted-octahedral coordination sphere. *Inorg. Chem.* **2013**, *52*, 4554–4561.
- (63) Lunghi, A.; Totti, F.; Sanvito, S.; Sessoli, R. The role of anharmonic phonons in under barrier spin relaxation of single molecule magnets. *Nat. Commun.* **2017**, *8*, 14620.